

Designing Metamaterial Cells to Enrich Thermoforming 3D Printed Object for Post-Print Modification

Donghyeon Ko

Department of Industrial Design,
KAIST
Yuseong-gu, Daejeon, South Korea
donghyeon.ko@kaist.ac.kr

Jee Bin Yim

Department of Industrial Design,
KAIST
Yuseong-gu, Daejeon, South Korea
jeebiny@kaist.ac.kr

Yujin Lee

Department of Industrial Design,
KAIST
Yuseong-gu, Daejeon, South Korea
neaj0812@kaist.ac.kr

Jaehoon Pyun

Department of Industrial Design,
KAIST
Yuseong-gu, Daejeon, South Korea
jhp960918@kaist.ac.kr

Woohun Lee

Department of Industrial Design,
KAIST
Yuseong-gu, Daejeon, South Korea
woohun.lee@kaist.ac.k

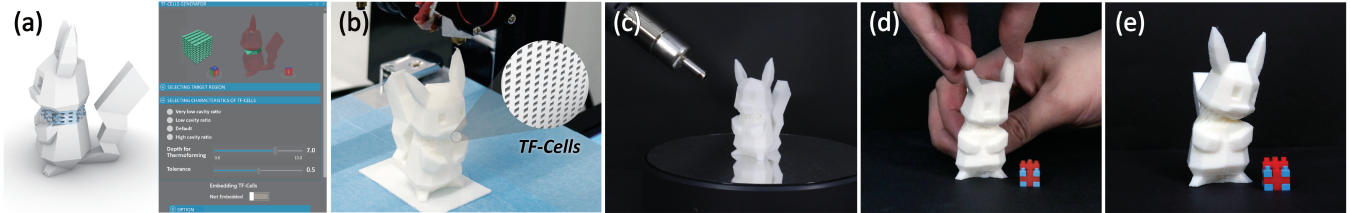


Figure 1: Thermoforming Low-Poly Pikachu through *TF-Cells*: (a) embedding *TF-Cells*, (b) printed object, (c) heating *TF-Cells*, (d) modifying shape of Pikachu (e) final appearance of Pikachu

ABSTRACT

In this paper, we present a metamaterial structure called thermoformable cells, *TF-Cells*, to enrich thermoforming for post-print modification. So far, thermoforming is limitedly applied for modifying a 3D printed object due to its low thermal conductivity. *TF-Cells* consists of beam arrays that affluently pass hot air and have high heat transference. Through heating the embedded *TF-Cells* of the printed object, users can modify not only the deeper area of the object surface but also its form factor. With a series of technical experiments, we investigated *TF-Cells*' thermoformability, depending on their structure's parameters, orientations, and heating conditions. Next, we present a series of compound cells consisting of *TF-Cells* and solid structure to adjust stiffness or reduce undesirable shape deformation. Adapting the results from the experiments, we built a simple tool for embedding *TF-Cells* into a 3D model. Using the tool, we implemented examples under contexts of mechanical fitting, ergonomic fitting, and aesthetic tuning.

CCS CONCEPTS

- Human-centered computing → Human computer interaction (HCI).

KEYWORDS

thermoforming, metamaterial, hands-on deformation, 3D printing, fabrication

ACM Reference Format:

Donghyeon Ko, Jee Bin Yim, Yujin Lee, Jaehoon Pyun, and Woohun Lee. 2021. Designing Metamaterial Cells to Enrich Thermoforming 3D Printed Object for Post-Print Modification. In *CHI Conference on Human Factors in Computing Systems (CHI '21), May 8–13, 2021, Yokohama, Japan*. ACM, New York, NY, USA, 12 pages. <https://doi.org/10.1145/3411764.3445229>

1 INTRODUCTION

Modifying a rigid 3D-printed object is challenging; users redesign and reprint a model to make alterations, thereby costing additional time and filaments. The printed object may also be heated for deforming it manually [10, 47]. In this regard, smoothing its surface, expressing textures, or even bending a part of it are possible through thermoforming [9, 12]. However, thermoforming 3D-printed objects is only applicable to thin objects or to a shallow depth beneath the surface. Owing to the low thermal conductivities of typical fused deposition modeling (FDM)-printed materials, heating deep and specific parts of printed objects is difficult. In a study, heating the objects through embedded electronics from the inside was suggested [10]. However, after heating, deforming the shape of printed objects could be restricted by the embeddings.

Permission to make digital or hard copies of all or part of this work for personal or classroom use is granted without fee provided that copies are not made or distributed for profit or commercial advantage and that copies bear this notice and the full citation on the first page. Copyrights for components of this work owned by others than ACM must be honored. Abstracting with credit is permitted. To copy otherwise, or republish, to post on servers or to redistribute to lists, requires prior specific permission and/or a fee. Request permissions from permissions@acm.org.

CHI '21, May 8–13, 2021, Yokohama, Japan

© 2021 Association for Computing Machinery.

ACM ISBN 978-1-4503-8096-6/21/05...\$15.00

<https://doi.org/10.1145/3411764.3445229>

We present a designed metamaterial structure, *TF-Cells*, with enhanced heat transference for an external heat source such as hot air. As *TF-Cells* are less dependent on geometry and heating direction, users can straightforwardly embed the cells into their 3D models (Fig 1. (a) and (b)) and heat them (Fig 1. (c)). Through this method, users can manually deform the printed object (Fig 1. (d)) in diverse manners, including modifying its surface or its form factor (e.g., modifying posture to face a certain direction like Fig 1. (e)).

In this paper, we firstly introduce the design space of thermo-forming *TF-Cells* and thermoforming through the cells. Second, we investigated characteristics of *TF-Cells* through technical experiments. Third, we present a series of compound cells to complement thermoforming through *TF-Cells* only. Finally, we present a simple tool for embedding *TF-Cells* and applicable contexts with examples.

Our primary contributions are as follow:

- We designed *TF-Cells* and compound cells for facilitating thermoforming;
- We characterized *TF-Cells* through a series of technical experiments;
- We implemented examples under applicable contexts using a simple tool.

We believe that this approach could invite a hands-on approach in digital fabrication from design to customization. Thereby, users can apply appropriate digital and tangible methods in overall design stages, leading to improved expressiveness and convenience. Moreover, they can design a specific part of an object while experiencing its physical properties such as the size, proportion, or form factor [23, 24].

2 RELATED WORKS

2.1 Hands-on Approach to Digital Fabrication

Adapting a hands-on approach to the digital fabrication process has been investigated in human-computer interaction (HCI) fields. One approach is to allow users to engage their hands in manipulating virtual models in the preprint stage [6, 11, 15, 48]. *MixFab* provides a modeling method using direct gestures that facilitates the incorporation of the physical object into virtual modeling [48]. Another approach is to engage users interactively in fabricating objects between physical and virtual spaces [25, 26, 29, 30, 40, 49]. For example, in *D-coil*, users can physically build a 3D model with the guidance of a digital system using wax coiling based on virtual models [30]. A few studies have investigated hands-on approaches in the post-print phase, particularly for deforming a 3D-printed object. *ReForm* allowed hands-on deformation of printed clay by globally heating shape of it in oven and synchronizing the deformed shape with the virtual model [47]. *Hotflex* embeds heating elements into local part of 3D-printed objects for customizing them. Depending on structural patterns, the printed objects can be diversely modified [10]. Distinctively, our metamaterial approach facilitates thermoforming through hot air. It allows relatively less restrictive deformation of local parts of 3D-printed objects without using electronics.

2.2 Embedding Structures into 3D-Printed Objects for Functional Purposes

Embedding the designed structures into 3D-printed objects has been adapted to include functionality. First, the excavated space inside printed objects can be used to embed interactive elements, such as a spring [13], optical fiber [50], conductive ink [34, 36], heating elements [10], or even smartphones [22]. Thus, the printed objects could be developed into shape-changing objects [43, 45], sensors [35, 36, 42], or even smart objects [22]. Another representative method is implementing metamaterial cell structures into 3D-printed objects. Ion et al. [16–18] presented a series of metamaterial concepts in digital fabrication. Without embedding any elements, metamaterial structures could perform directional deformation [16], digital logics [18], and transformable textures [17]. A similar approach is followed in designing repetitive structures for facilitating the thermoforming process of 3D-printed objects.

2.3 Shape-changing through Heating

Heating has been extensively applied to change shapes in digital fabrication. It allows users to deform rigid objects for iteratively designing or customizing [10, 14, 26, 47] them. Also, heating triggers self-actuated shape-changing to pre-programmed shape through folding [3, 33, 38, 41, 46], shrinking [39], and expanding [19], called 4D printing. In *Meltables*, objects with a joint-and-beam structure are self-deformed due to gravity when the joints are heated [33]. Using shape-memory nature of poly lactic acid (PLA), heat-triggered self-folding objects can be implemented with conventional FDM printer as *Thermorph* presented [3]. Similarly, *A-line* presented the heat-trigger self-folding 3D-printed line [46]. Moreover, 4D printing approach has been rigorously used to design heat-actuated textures [38] or heat-actuated fitting by shrinking [39]. In contrast to the various uses of heating, their approaches would be restricted by the low thermal conductivity of materials. Considering that most of them use hot air or water as the actuating source, control of the thermal conductivity in our method might presumably contribute to enhance their approach.

3 THERMOFORMABLE CELLS: ENRICHING THERMOFORMING OF POST-PRINT MODIFICATION

Thermoforming has been used to form shapes from thin thermoplastic materials which soften by heating (they become highly viscous fluids). Therefore, thermoforming allows post-print modification of 3D-printed objects [10]. We illustrate possible ways of thermoforming which are applicable to 3D-printed objects referring to previous cases [9, 10, 12, 37, 47] and ideation workshops with 5 designers, 2 makers, and 3 engineers (Figure 2). First, thermoforming enables modification of an object surface. After heating, smoothing a surface, as in ironing, has been used for surface finishing. Further, joining other objects is possible after heating surfaces for repair or assembly [10]. Users can also express textures into a surface like hair-line or skin textures [12]. Designers can iterate rounding edges through filleting. While thermoforming deep areas of an object, users can easily copy specific shapes or physical patterns through stamping [37]. In addition, they can roughly measure and then fit

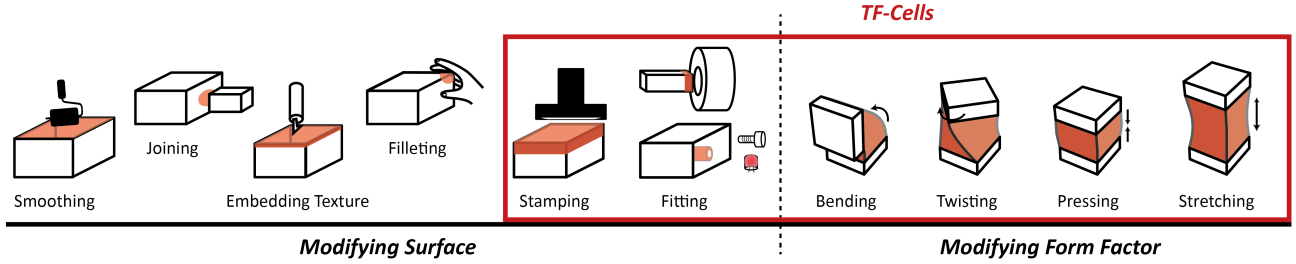


Figure 2: Possible thermoformings applicable to 3D-printed objects for modifying surfaces and form factors

the printed objects into other objects or embed external objects into the printed object [9, 10]. Moreover, when a section of body is heated, users can modify the form factor of printed objects. By modifying (i.e., stretching, pressing, bending [9, 10, 12], and twisting) the heated and thus malleable sections, users can iteratively explore the size or proportions of the object or customize its overall shape.

Thus far, these thermoformings are limited in their abilities. Modifying surfaces (stamping and fitting) or form factor requires heating specific and deep areas of the object; otherwise, unintended parts can melt. Regarding this, the designed *TF-Cells* could facilitate them as the high heat transference of the cells allow to heat deeper and specific areas. In the following sections, we describe the design of *TF-Cells* and how they can be used in thermoforming.

Throughout this paper, we focus on external heating using a heat gun and poly-caprolactone (PCL) filament for the printing material. A heat gun is feasible for controlling the temperature and airflow. The PCL filament (*eMate* from *eSUN*) has a low melting temperature of 60 °C. Therefore, at this melting temperature, PCL is safe and feasible for hands-on deformation [1, 10]. For printing, we used Creality Ender 3 with a 1.75 mm nozzle size. We used the default CURA setting of 0.2 mm of layer height and 0.4 mm of path width. A printing speed of 18 mm/s and nozzle temperature of 87 °C were used. To print at low temperatures, the cold extrusion lock from *Marlin Firmware* was discarded.

3.1 Design of Thermoformable Cells

Metamaterial structures have been rigorously studied to achieve intended properties including thermal properties [31]. They primarily use methods of combining materials with distinctive thermal conductivity (e.g., copper and vacuum) to control the bulk thermal conductivity. With different arrangements, the heat transference and heat flux can be varied [28, 32, 44]. To facilitate thermoforming 3D-printed objects, we adapted this principle by designing highly

heat-transferable structures and combining them with conventional structures having low thermal transference. We adopt the following design considerations for our structure:

- Enhanced heat transference: It is essential for the structure to have distinctively high heat transference compared to those of conventional structures to allow heating specific and deep areas;
- Printability: The structure should be printable with moderate quality when embedded into most geometries;
- Heating in multiple directions: The structure should transfer heat from multiple directions unless the heating direction is largely constrained depending on the embedding orientation and position;
- Structural robustness: A minimum mechanical strength for typical contexts should be guaranteed after embedding the structure.

To increase the heat transference, we start with a perforated structure which has been adapted for controlling the light or sound [7]. Unlike the low thermal conductivity of air ($k_{PLA} : 0.13$, $k_{ABS} : 0.25$, $k_{PCL} : 0.2$, $k_{air} : 0.026 \text{ W/m}^{-1}\text{K}^{-1}$ at 27 °C), the perforated cavity becomes a channel for air flow that increases heat transference of the printed object.

According to heat simulation results, when heated through hot air using a heat gun, perforated structures exhibit higher temperature distribution from front to back than that of non-perforated structures (Fig 3. (a)). Among perforated geometries, we used a beam array as the primitive structure. This is because, as illustrated in (Fig 3. (b)), when the beams are parallel (α array), the airflow can pass between beams (gap). Moreover, as the extruded line fills every geometry's inner structure in FDM printing, a beam array could easily be embedded into most geometries and be printable. To embed it into a 3D object, we expanded 2D beam array to a 3D array. To pass the air in three axial directions, we stacked beams

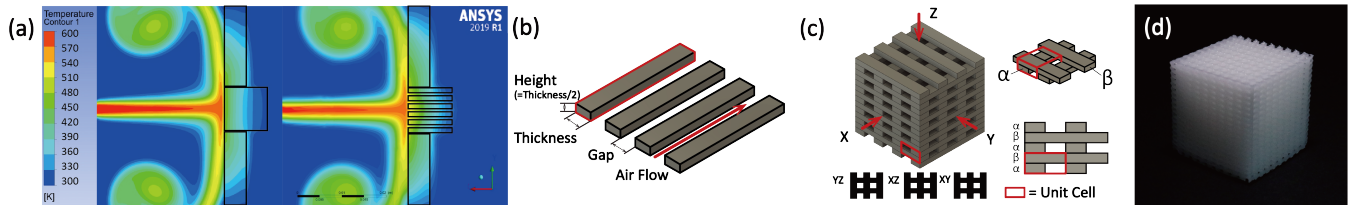


Figure 3: (a) Heat simulation results, (b) Primitive beam array, (c) Designed *TF-Cells*, (d) Printed *TF-Cells*

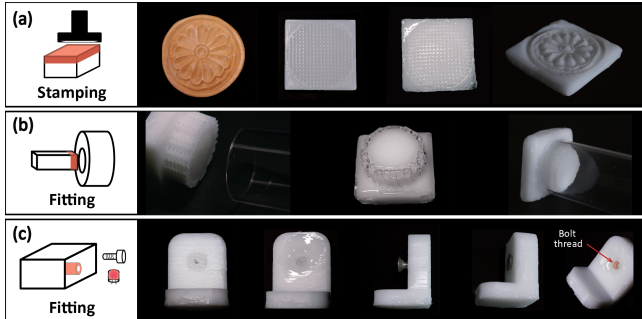


Figure 4: Thermoforming through *TF-Cells* for modifying a surface: (a) stamping flow pattern, (b) fitting a 3D-printed object to a pipe, and (c) fitting a bolt to a 3D-printed object

in a perpendicular direction (β array) to the existing α arrangement layer for the upper layer. We call this repetitive α - β array *Thermoformable Cells* (*TF-Cells*) (Fig 3. (c) and (d)).

For *TF-Cells*, the size of a beam and gap are decisive factors in controlling the size of unit cells, appearance, and thermoformability (i.e., the degree of being heated and thus deformed) of the printed object. We set the height as a half of the thickness of a beam which follows the proportion of the extruded line's height to its width in general FDM printing. A unit cell size of *TF-Cells* is $(\text{thickness} + \text{gap}) \times (\text{thickness} + \text{gap}) \times (\text{thickness})$. The ratio of cavity in a unit cell is $\frac{\text{gap}}{\text{thickness} + \text{gap}}$, called cavity ratio. The effects of gap and thickness will be covered in the technical experiments section.

3.2 Thermoforming through *TF-Cells*

Thermoforming through *TF-Cells* requires only a few steps. The first step is embedding *TF-Cells* into a target part of the 3D model. With hot air, users can specifically heat the cell-embedded parts into a malleable state, differentiated from other regions. During heating, the deformable state is identifiable because PCL material becomes transparent near its melting temperature. Thereby, users can freely deform the malleable target part until the part cools down. We describe how to apply the designed *TF-Cells* to stamping and fitting when modifying surface, or bending, twisting, pressing, and stretching when modifying form factor.

3.2.1 Modifying Surfaces: Stamping and Fitting. Stamping the surface of 3D-printed objects is achieved simply through embedding *TF-Cells* into an object's surface, heating it, and stamping it. To copy the flower pattern (Fig 4), we embedded *TF-Cells* into a rectangular object ($63 \times 63 \times 12\text{mm}$). The cells were embedded in a circular shape (diameter: 58 mm) slightly bigger than the stamp (minimum/maximum diameters: 49/56 mm, pattern depth: 3.5 mm), and 4 mm deep. We heated the whole surface from the top of the

printed object, which becomes transparent when it is in the malleable state, as in Fig 4. (a). Through stamping the cell-embedded area, we could reproduce the copied shape. As cavities in the *TF-Cells* condense, the stamped surface does not get perforated. We recommend embedding the cells into a slightly larger and deeper area (by approximately 120%) than the stamping pattern itself considering the volume reduction.

Embedded *TF-Cells* provide a space for fitting. We implemented two fitting scenarios, fitting a printed object into a pipe and fitting a bolt into a printed object. Considering the pipe's inner diameter (25 mm), we embed *TF-Cells* fill the 4 mm depth around the circle area (diameter: 23 mm). After heating, we could tightly fit the object into the pipe (Fig 4. (b)). To put a bolt (diameter: 5 mm) into the printed object, we embedded the cells into a 5.5 mm square area at the object's side and made a circular hole (diameter: 2 mm) at the center of the square. As the bolt length was 5 mm, we embedded *TF-Cells* 7 mm deep. After heating the target area, we could successfully fit and fully insert the bolt (Fig 4. (c)). After this, the surface was made to match the thread from the bolt. We recommend providing empty space or using a large depth of the cells (130 to 150% of an inserting object's length) for embedding external objects.

3.2.2 Modifying Form Factor: Stretching, Pressing, Bending, and Twisting. Modifying the form factor of a printed object becomes possible with *TF-Cells*, which allows users to customize or iterate its overall shape. We embedded *TF-Cells* into a ($15 \times 15 \times 20(\text{mm})$) section of a cuboid. This cuboid was modified by deforming *TF-Cells* like a joint. We heated that section primarily from the front and back and briefly from other directions. Then, we could easily modify the cuboid shape.

As illustrated in Fig 5. (a), we stretched *TF-Cells* into 30 mm. When stretching the object, the stretched parts become narrowed (necking). Thus, we could not elongate the object more than 40 mm because the section might become too narrowed or fractured. The malleable *TF-Cells* could be easily pressed, reducing the overall length. When the height of *TF-Cells* becomes a half (10 mm), the pressed volume overflows from the pressed parts as shown in Fig 5. (b). It is possible to bend the printed object over 90° . However, after bending, the cross-section of the pressed side became widened with excess mass, as in the case of pressing (Fig 5. (c)). The opposite side narrowed, as in stretching. Twisting was also easily possible. We could twist the object for five full turns without constraint, as in Fig 5. (d).

Users need to modify the shape carefully so as not to distort or fracture it as it is almost unconstrained in its malleable state. It should also be held for approximately two minutes after modifying the shape until it becomes slightly rigid. We recommend not heating the object beyond 100°C because the heated parts become considerably weak.

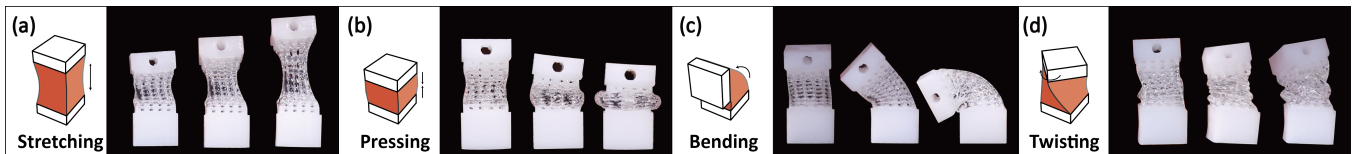


Figure 5: Thermoforming through *TF-Cells* for Modifying Form Factor: (a) stretching, (b) pressing, (c) bending, and (d) twisting

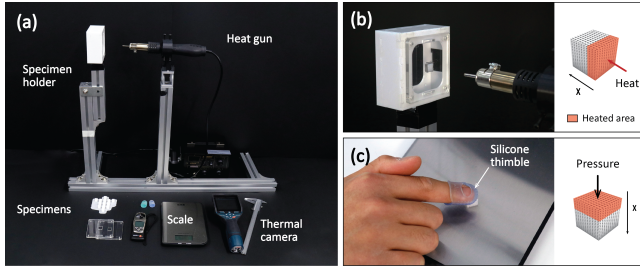


Figure 6: (a) Experimental setup, (b) Heating a specimen in the holder, (c) Pressing the specimen with 20 N force using a scale

4 INVESTIGATIONS OF TF-CELLS WITH TECHNICAL EXPERIMENTS

We investigated *TF-Cells* through a series of technical experiments, which are described in this section. The experiments reported 1) thermoformability of *TF-Cells* depending on structural parameters, orientation, and heating condition, 2) mechanical strength of *TF-Cells*, and 3) effects of malleable state and cavity ratio on the four shape modifications. The results provide useful guidelines for using *TF-Cells*.

4.1 Experiment 1: Thermoformability of *TF-Cells*

As a perforated structure passes air, it is presumed that all perforated structures could be made malleable through heating. However, there was a limitation, as heated parts spread and block the front cavity. In the initial experiment, we evaluated how deep *TF-Cells* are heated and thus deformed in a malleable state through various *thickness* and *gap*. For comparison, conventional printing structures (100% infill (*Solid*) and a 40% infill (a grid type) with solid wall, default setting of CURA (*Conventional*)) were also tested. Considering a printer's path width of 0.4 mm, we varied the cells' thickness in 0.4 mm intervals, from 0.8 mm to 2.4 mm, and half intervals (0.2 mm), from 0.6 mm to 2.4 mm, for the gaps. We used small cuboids of $10 \times 15(\text{depth}) \times 10\text{mm}$ that included at least 72 unit cells (with 16 at the front) as maximum thermoformed depth was less than 12 mm.

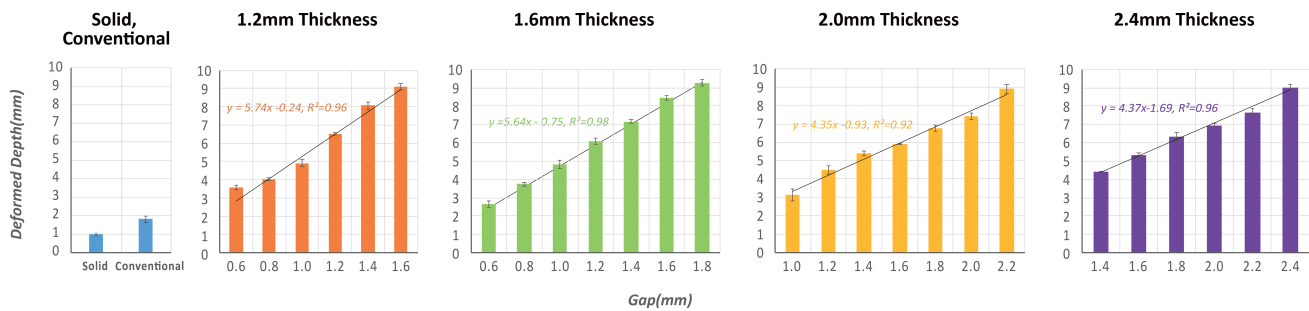


Figure 7: Deformed Depth of *TF-Cells(X)* with different thickness and gap and fitting curves

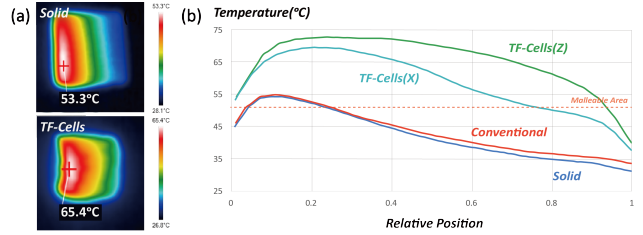


Figure 8: (a) Thermal image of the side of the *Solid* and *TF-Cells* specimens along the Z-direction, *TF-Cells(Z)*, (b) cross-section showing the temperature distribution across the various specimens (0 is the front and 1 is the back)

The experimental setup is illustrated in Fig 6 (a) and (b). First, assuming that the cells are embedded into a bulk object, the specimen was placed in a specimen holder. Only anterior parts of the specimens were heated with hot air (a 3 mm diameter nozzle 60 mm away from the specimen, inner temperature of heat gun: 200 °C, air speed at the front: 1.1m/s) where the front part of the specimen does not collapse from melting or air flow (the details are elaborated in further sections). After heating, we measured the temperature of the specimen with a thermal camera (Bosch G400C Pro) and pressed the specimen with approximately 20 N of pressure for 5 s, as shown in Fig. 6 (c). As deforming an object with larger force (>20N) is not adequate for a minute or more [20], we regarded the specimens undeformed by 20 N-force as not deformable. As heated parts are centralized and relatively irregular, as shown in Fig 8. (a), we used a soft finger thimble to apply pressure on the parts. Concurrently, the majority of malleable mass moved into cavities or out of a specimen, and thus, the deformed mass near the deepest part was less than 0.1 mm. Finally, the deformed depth of the deepest point was measured. However, because it was manually pressed and measured, the deformable depth might have an error. To compensate for such errors, each condition was evaluated four times with freshly printed specimen. During the experiments, the room temperature was maintained close to 24 °C.

4.1.1 Results and Findings. As thermal images show (Fig 8. (a)), *TF-Cells* could be heated further. Temperature distributions of the specimens (Fig 8. (b)) show that *TF-Cells* along both the X- and Z-axes (*TF-Cells(X)*, *TF-Cells(Z)*) have higher temperatures in all positions than those of *Conventional* or *Solid*. Evidently, *TF-Cells(X, Z)* have larger deformable depths than the others, as visualized

in Fig 8. (b) (the malleable area is from 0 to the point where the temperature line intersects the orange dotted line). Concurrently, *Solid* demonstrated a lower deformed depth (1.0 mm, SD: 0.3) than *Conventional* (1.8 mm, SD: 0.1). Considering that *Solid* has no cavities unlike *Conventional*, dense *Solid* is an impeding factor because it absorbs heat from the hot air.

We extensively evaluated thermoformability of *TF-Cells(X)* which have an inferior thermoformability than that of *TF-Cells(Z)* according to gap and thickness. We present the data consisting of 4 *Solid* specimens, 4 *Conventional* specimens, and 124 *TF-Cells* specimens as illustrated in Fig 7. For *TF-Cells* specimens, we only analyze the dimensions which exhibit a moderate printing quality and non-structural collapse during heating. The results account for the thermoformable depth depending on the structural parameters of the cells. When a gap increased, the deformed depth also increased. The opposite occurred, however, when the thickness increased. During heating, the malleable anterior parts spread, blocking the cavities (i.e., the air path). Therefore, a small gap could be quickly blocked. On the contrary, increasing thickness decreases the deformed depth as the larger area of deformable mass both blocks the cavity area and absorbs more heat. However, a small thickness or large gap decreases the printing quality. In our case, a thickness less than 0.8 mm exhibited unstable printing results. When the gap was larger than the thickness, the structures largely collapsed or shrunk during heating (e.g., 1.2 mm thickness and 1.8mm gap). In addition, beyond 2.0 mm gap, some specimens' cavities were irregular due to bridging problems. Considered all, 10 mm seems to be maximum deformable depth when heating in a single direction. As heating in multiples directions and emptying the inner part are possible, thermoforming larger objects would be feasible. We fit 1st order polynomial curves on the resulting data for each dimension of thickness ($R^2 > 0.9$), which were used to specify the dimension of *TF-Cells*, especially in the design tool. Based on a rule of thumbs, 1.6 mm thickness (t) and 1.4 mm gap (g) were appropriate for *default* parameters to use in a universal situation considering moderate thermoformability, appearance (appears insufficiently perforated), and favorable printing quality.

4.2 Experiment 2: Thermoformability with Orientations

Certain geometries are hard to heat along perforated directions (X, Y, and Z) of *TF-Cells*, such as when the cells are embedded into the side section of a cylinder. For such cases, the thermoformability of *TF-Cells* according to their orientation could provide a reference to set the dimensions of the *TF-Cells*. We varied the specimens at 15° intervals to test the effect of orientation on the thermoformability, as shown in Fig 9. (a). The testing specimen was a 30×30×30(mm) cube with *default* *TF-Cells* (1.6 t and 1.4 g (mm)). Our heating condition was 200 °C with an air flow of 1.1 m/s for 130 s. Each condition was tested three times with freshly printed specimen. The results are illustrated in Fig 9. (b).

4.2.1 Results and Findings. 0° orientation exhibited the largest deformed depth (average 7.2mm). 45° orientation showed the least deformed depth, which was 1.5 mm lower than that of 0° orientation. Although air can pass through the cavities at 45° orientation, its structure is slightly vulnerable to being blocked. Therefore, when

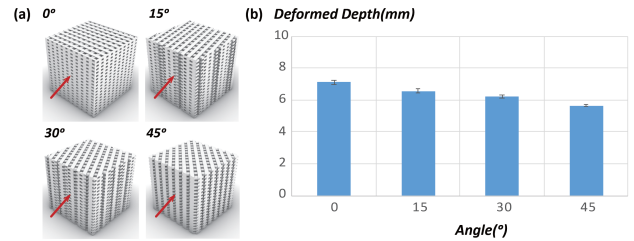


Figure 9: (a) Embedded *TF-Cells* in different orientation (b) deformed depth according to orientations

heating in a straight direction is difficult, we recommend to conservatively set dimension of *TF-Cells* (i.e., use more gap to achieve the desired thermoformable depth). We adopt this result to tool by allowing to set *tolerance*.

4.3 Experiment 3: Thermoformability according to Heating Condition

We examined effects of heating condition on *TF-Cells* which could be referred for actual use. For this test, a 30 mm cube filled with *default* *TF-Cells* was used as the test specimens. It was heated for 5 min to observe changes in the appearance of *TF-Cells* until after the cavities were blocked. We varied air speed (from 0.9 to 1.5 m/s) and temperature (from 100°C and 0.9 m/s to 250°C) with a fixed distance (60 mm away from the specimen). Each condition was tested three times with freshly printed specimen.

4.3.1 Results and Findings. When the temperature is relatively low (100°C and 150°C) increasing the airflow speed can heat further, as shown in Fig 10. (a). In contrast, in the case of 200°C and 250°C temperatures, increasing the airflow speed decreased the deformed depth. For example, compared to an airflow speed of 0.9 m/s at 250°C, 1.1 m/s at 250°C shows a shallower depth. The reason is related to the spread of the malleable mass. When the temperature is high, the mass becomes quickly malleable, but simultaneously, it becomes vulnerable to spread by airflow which blocks the cavity. In this experiment, the optimal heating condition was 200 °C with a 1.1 m/s airflow speed for approximately 120 s which is balanced between airflow and temperature. We recommend using high temperature with slow airflow speed referring to our heating conditions. When heating along different distance, the results could be also applicable considering that as the distance decreases, the airflow speed and temperature at the target position increase.

We illustrated the 250°C, 1.3 m/s case, which advances from being malleable to being melted down, in Fig 10. (b). Initially, hot air passes through the cavities. Concurrently, the front *TF-Cells* appear to be expanded (spread by air flow). At approximately 120 s, the front cavities become fully blocked. This state was recommended as the appropriate state for forming. For certain period, the appearances remains relatively unaltered. At approximately 200 s, the anterior parts start to melt down or become largely deformed by air flow. Finally, they become fully transparent and the geometry of the printed object is melted down at 300 s. Unlike Experiment 1 results (200°C, 1.1 m/s, 130 s), five minutes of heating (200°C, 1.1m/s) exhibits a slightly higher deformed length of approximately 1.2 mm.

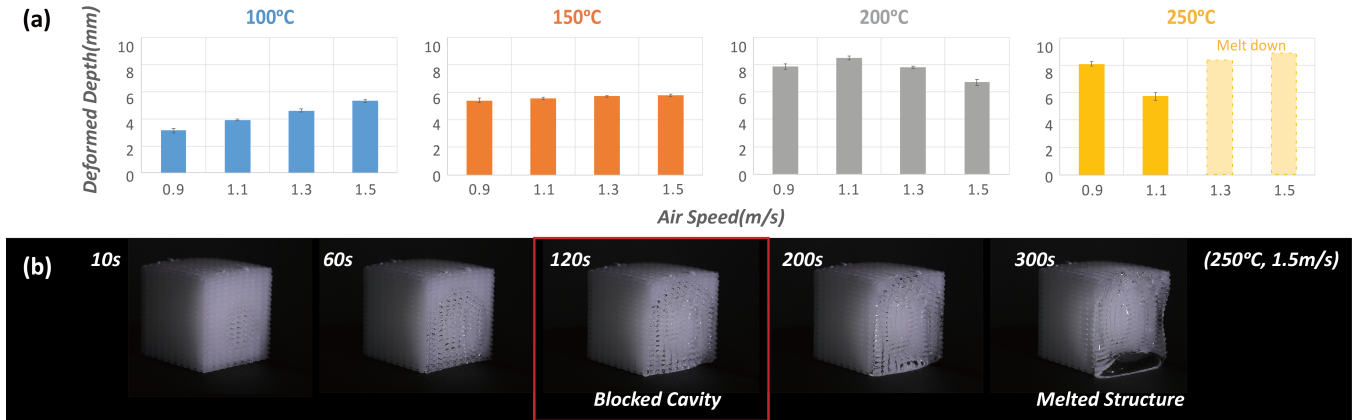


Figure 10: (a) Deformed depth according to heating conditions (b) Heating TF-Cells with 250 °C with 1.5m/s airflow speed

However, the overall structure could be melted down (like Fig 10.(b)). This state is not appropriate for forming as the mass become extremely sticky and weak to deform or to sustain a deformed shape.

4.4 Experiment 4: Mechanical Strength of TF-Cells

As TF-Cells are a perforated structure without a shell, its strength might be less than that of normal structure. We examined the mechanical strength of TF-Cells for validating structural robustness. Tensile tests were conducted with the universal test machine with 15 mm/min displacement speed. The specimens included Solid, Conventional, and default TF-Cells.

4.4.1 Results and Findings. TF-Cells had sufficient strength similar to that of concrete (4.9MPa) for typical use. Tensile strengths of TF-Cells(X) and TF-Cells(Z) were 5.69MPa (SD: 0.69) and 5.59MPa (SD: 0.10), respectively. They were lower than both Solid (15.2MPa, SD: 1.08) and Conventional (9.51MPa, SD: 0.10). Notably, when the cells were heated and pressed into -0.5 strain, parts of the TF-Cells become dense like a solid, which resulted in approximately 6.86MPa tensile strength. On the contrary, when the cells were stretched with a 0.5 strain after heating, the strength was reduced to approximately 2.94MPa. As the cross-section of stretched cells decreased, the sustainable weight decreased.

4.5 Experiment 5: Shape Modifications through TF-Cells

As previously shown, the overall shape of 3D printed objects could be modified through stretching, pressing, bending, or twisting the heated TF-Cells. For the modifications, malleable state of TF-Cells and the cells' cavity ratio are decisive factors in requiring force and defoformable range, and deformed appearance respectively. First of all, we compared each modification in fully malleable state with in partly malleable state using two types of specimens 15 × 15 × 20(mm) and 20 × 20 × 20(mm) filled with default TF-Cells, called 15 mm TF-Cells and 20 mm TF-Cells in each. Considering the thermoformable depth of default TF-Cells was around 7.2 mm, only 15 mm TF-Cells would be fully malleable after heating in multiple

directions. For comparison of different cavity ratios, we used 15 mm TF-Cells with 1.2 t and 1.3 g (mm), and 2.4 t and 2.0 g (mm) which have distinctive cavity ratios of 0.52 and 0.45 in each but have similar thermoformable depths (approximately 7 mm).

Our heating conditions were 200 °C of heat gun temperature, 1.1 m/s of airflow (at the front of the specimen), and 60 mm distance from the heat gun. We gradually rotated the specimens (at 1.71 RPM with NEMA 17 stepping motor) for 5 min with a turn-table, as illustrated in Fig 11. (a). Through several trials, we discovered that this duration of rotation was sufficient As 15 mm TF-Cells become fully malleable while retaining their original structure. Deformation methods are illustrated in Fig 11. (b). We used 1 N, 5 N, 10 N, and 20 N weights for the stretching, pressing, and bending tests. For the twisting, we applied 0.31N · m after with clamping the top section of the specimen. Next, to compare deformed appearance of TF-Cells with different cavity ratios, we stretched specimens to 40 mm from 20 mm height of TF-Cells, bended them to 90°, twisted five full turns, and pressed them with 1 N. We repeated each deformation test three times .

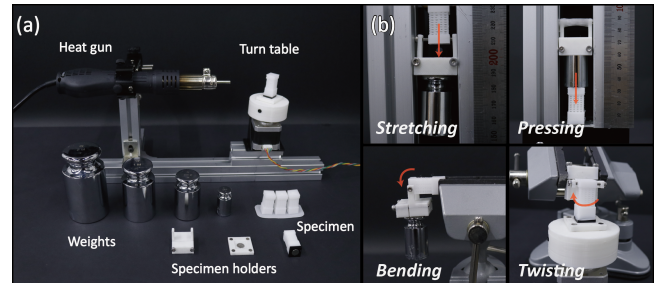


Figure 11: (a) Experiment setup (b) Deforming Methods

4.5.1 Result and Findings: different degree of malleable state. After heating, the middle parts of 20 mm TF-Cells specimens remained un-malleable (average non-malleable area: $7.3 \times 7.3(\text{mm}^2)$, SD: 0.3 for a side length). As a result, 20 mm TF-Cells were not deformable during stretching and pressing, and they only partially bent and twisted, while 15 mm TF-Cells were deformed in all deformation tests with 1 N.

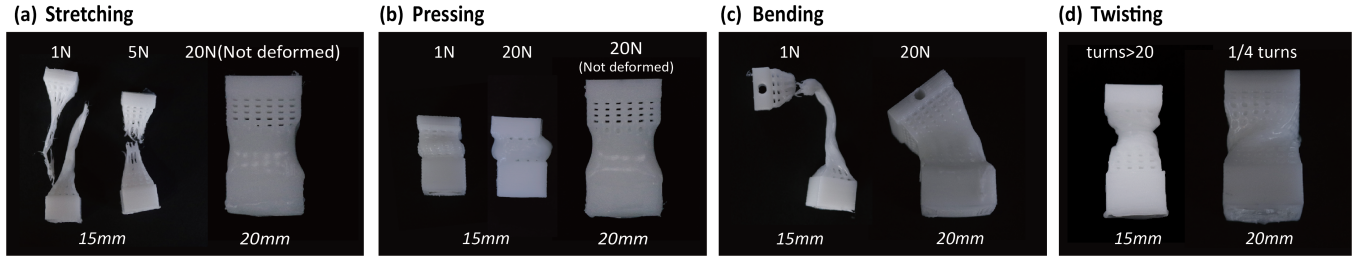


Figure 12: Modified shape in a different malleable state: (a) stretching, (b) pressing, (c) bending, (d) twisting

15 mm *TF-Cells* were stretched with necking and eventually cut off as illustrated in Fig 12. (a). Specimens were less stretched and quickly (less than a second) cut off with 5 N weights, while 1 N weights rather slowly lengthened (for approximately 3 s) the specimens. In case of pressing, 15 mm *TF-Cells* were pressed using -0.46 strain (SD: 0.03) with 1N and -0.59 strain (SD: 0.03) with 20 N (Fig 12. (b)). 15 mm *TF-Cells* was bent more than 90° with a 1 N weight, then slowly stretched, and finally cut off (Fig 12. (c)). Finally, 15 mm *TF-Cells* were twisted with minimal resistance regardless of the angle. When they rotate more than 6 turns, their central parts were cut off (Fig 12. (d)). Although fully malleable parts could be deformed with little resistance, they should be carefully deformed with minimum force to avoid distortion or fracture.

To stretch and press the heated *TF-Cells*, the entire part should be malleable, or non-malleable parts need to be fractured. As 20 N was not enough for breaking the parts, 20 mm *TF-Cells* were not stretched and pressed at all. On the contrary, in the case of bending and twisting, the non-malleable parts lead to stiff deformations. 20 mm *TF-Cells* were bent approximately 50° with 20 N and twisted by approximately 90°. Notably, the non-malleable parts showed elastic properties by slightly returning to their original shapes [4, 5]. This indicated the necessity of complementing *TF-Cells* in shape modifications which is covered in the next section.

4.5.2 Results and Findings 2: different cavity ratio. Overall, *TF-Cells* with a lower cavity ratio exhibited less narrowed widths for stretching but more excessive mass for other deformations. After stretching, *TF-Cells* with 2.4 t, 2.0 g (mm) exhibited less narrowed width from necking (strain: -0.29, SD: 0.05) compared to widths of the other (strain: -0.47, SD: 0.02)(Fig 13. (a)). When pressing with 1N, *TF-Cells* with 2.4 t, 2.0 g (mm) was less pressed (strain:-0.41, SD: 0.02) than the other (strain:-0.55 SD: 0.02) (Fig 13. (b)). After bending, *TF-Cells* with 2.4 t, 2.0 g (mm) exhibited less narrowed width (strain:

-0.27, SD: 0.03) and larger width from excessive mass (strain: 0.10, SD: 0.04) than the other's narrowed width (strain: -0.45 strain, SD: 0.02) and enlarged width (strain: 0.02, SD: 0.05) (Fig 13. (c)). After twisting *TF-Cells* with 2.4 t, 2.0 g (mm), bulk mass rotated together and slightly moved down, while twisting made the middle section of *TF-Cells* with 1.2 t, 1.3 g (mm) become a condensed column, as shown in Fig 13. (d).

Except for twisting, *TF-Cells* with low cavity ratio would be adequate for large elongations (e.g. stretching and bending short objects) as it would be less fractured. In contrast, *TF-Cells* with a higher cavity ratio would be appropriate for large volume changes such as pressing and bending long objects (also recommended for stamping and fitting).

5 COMPOUND CELLS: THERMOFORMABLE CELLS WITH SOLID

In metamaterial research, combining different cells with distinctive properties, compound cells, can be optimal for specific functions [16]. We made compound cells to expand on thermoforming using only *TF-Cells*. From technical Experiment 5, we discovered that non-malleable parts can be used for providing resistance to deformation. Inspired by this, we embedded *Solid*, which exhibits inferior thermoformability, into *TF-Cells*. Using *Solid* in *TF-Cells* has two purposes: provides a resistance when deforming *TF-Cells* and blocking the movement of any malleable mass. We attempted various *Solid* geometries combined with *default TF-Cells* and present promising examples of compound cells, focusing on giving constraints and preventing undesirable deformed appearance.

5.1 Examples of Compound Cells

5.1.1 Simple Beam: adding stiffness to bending and twisting. Although *TF-Cells* are easily bent, the lack of stiffness can lead to

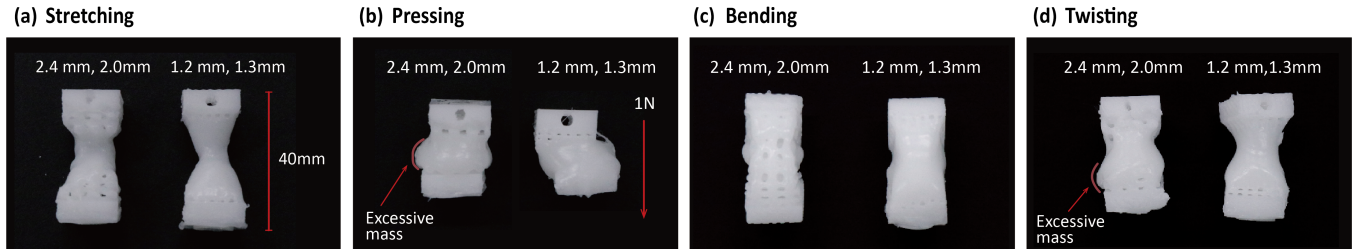


Figure 13: Modified shape with different cavity ratios for: (a) stretching, (b) pressing, (c) bending, and (d) twisting

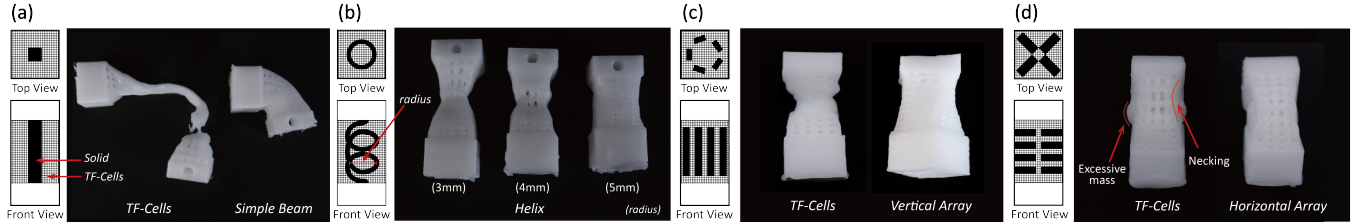


Figure 14: Compound cells with schematic view: (a) Simple Beam, (b) Helix, (c) Vertical Array, (d) Horizontal Array

distortion or difficulty in achieving the precise bending angle. We present a representative combination, *Simple Beam*. We embedded Solid with beam geometry (cross-section: $3 \times 3\text{mm}^2$) into *TF-Cells*, as illustrated in Fig 14. (a). When heating, *Simple Beam* becomes a flexible axis that gives additional stiffness. Thus, up to 5 N, it could be bent approximately 90° without fracturing. This structure is also adaptable for twisting.

5.1.2 Helix: adding stiffness and reducing necking when stretching. When stretching malleable *TF-Cells*, necking occurs and the cells can be cut off. *Simple Beam* is not adaptable for stretching as beam shape of *Solid* within *TF-Cell* will only elongate slightly. We embed a helical *Solid* into *TF-Cells* called *Helix*, which is sufficiently flexible for stretching. The pitch and turn of the spiral should be adjusted according to the length of the target region (we used 2.5 turns for 20 mm height) or else it would be same as a simple beam. We varied the radius of the spiral (3, 4, and 5 mm) with a 1.2 mm radius of cross section. As seen in Fig 14. (b), while a larger helix radius stiffens the cells leading to a shorter elongation, a smaller helix radius exhibits more elongation with less stiffness. This is because a helix having a large radius interferes with the cells being heated inside. For the 3 mm radius, the specimens could be stretched until a strain of 0.27 using 1 N of weight without being cut off.

5.1.3 Vertical Array: uniform deformation when twisting. During twisting *TF-Cells*, central parts rotate, while upper and lower parts are not rotated. To uniformly twist a part, we designed a vertical array by embedding a circular array of vertically long *Solid*, called *Vertical Array*. As shown in Fig 14. (c), the specimen became rather evenly twisted along the edge line because each vertically long *Solid*s distribute torsion. Further, *Solid* column shields some portion of the hot air which makes the twisting stiffer. For the vertical array, radius of the circular array and dimension of the *Solid* are decisive parameters.

5.1.4 Horizontal Array: relieving undesired deformation when bending. When bending *TF-Cells*, both necking in the elongated parts and excess mass in the pressed parts were observed. To resolve these issues, we embedded horizontal beam array, where a stack of angled *Solid* cross shapes are arranged, called a *Horizontal Array* as shown in Fig 14. (d). The array of *Solid* sections blocks any excessive mass movement and reduces necking. Unlike bending *TF-Cells* only (strain of narrowed width: -0.26, SD: 0.05), the narrowed width after bending the *Horizontal Array* was only 1.4 mm (strain: -0.09, SD: 0.03). In addition, as with the *Vertical Array*, it showed increased stiffness. For *Horizontal Array*, the gap between the cross shapes, position of, and height of the cross shapes need to be controlled so

as not to block *TF-Cells*' cavities. Also, we recommend to control the shape height from 1.2 mm unless it is not effective.

Thus far, several examples of compound cells that could relieve appearance issues and the lack of stiffness when modifying shapes have been presented. Several possible combinations remain undiscovered such as different shapes of *Solid* and its parameters, and replacing *Solid* as an empty space with various shapes. In addition to relieving these issues, controlling heat flux or guiding deformations might be achieved.

6 IMPLEMENTATION OF TF-CELLS WITH A SIMPLE TOOL

We built a simple tool for easily embedding *TF-Cells* into 3D objects with Grasshopper 3D and its components. The tool consists of two steps: selecting the target part and deciding characteristic of *TF-Cells*. First, users enter a target 3D model and draw a rough 3D geometry as in Fig 15. (a). The overlapped region between the target model and the drawn geometry becomes the target region that the tool replaces as *TF-Cells*, as shown in Fig 15. (c). Next, users select the characteristics of *TF-Cells* and click the embed button. By incorporating the experimental results, we focused on thermoformable depth (the fitting curves from experiment 1), setting *tolerance*, cavity ratio resulting in a section for setting the cells' characteristics as Fig 15. (b). To be specific, depending on modifications and the geometry of a model, we allow to set the cavity ratio in four levels (High cavity ratio (1.2 mm thickness) to very low cavity ratio (2.4 mm thickness)), the desired thermoformable depth and *tolerance* of the target depth. Then, the tool derives the thickness and gap size for the *TF-Cells*. Finally, the tool replaces the selected region of a 3D model with the specified *TF-Cells*. Currently, to implement the compound cells, the *Solid* shape is manually inserted into *TF-Cells*. For printing, user can use any slicing tool like CURA with default

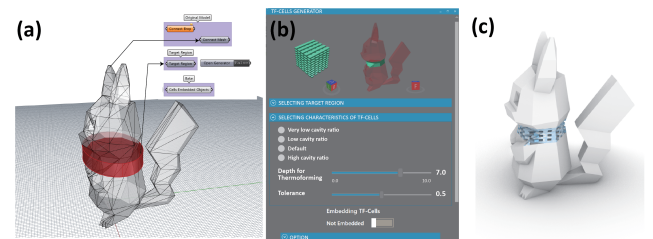


Figure 15: Design tool: (a) setting base 3D model and a target region, (b) setting *TF-Cells* characteristics, (c) the cell-embedded model

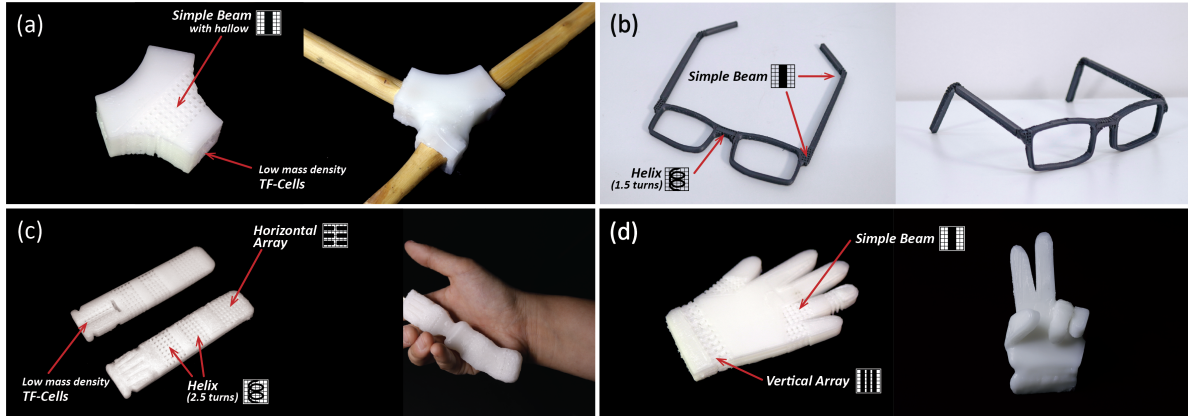


Figure 16: Application examples: (a) three-way joint, (b) glasses, (c) screw gripper, (d) peace hand gesture

settings except for increasing *Wall thickness* and *Top/Bottom thickness* to 2.4 mm. This setting results in the cells being surrounded by *Solid* for selectively heating the target area.

Thus far, this tool is in a nascent stage. As the next step, automatically setting the characteristics of *TF-Cells* depending on the purpose of modification, implementing compound cells, and making inner parts of *TF-Cells* hollow for large geometries will be considered.

7 APPLICATIONS

As previously shown, *TF-cells* allow stamping, fitting, and modifying a shape. Considering the modifications, *TF-Cells* have strong points for rough measuring for fitting, modeling for easy print, customizing and simplifying modeling. Taking these advantage, several examples were implemented under mechanical fitting, and ergonomic fitting, and aesthetic tuning with our tool.

7.1 Mechanical Fitting: three-way joint

Thermoforming through *TF-Cells* enables deforming shape of a section of an object while retaining core parts. Although there are several universal 3D-printed joints for DIY furniture, customizing to a personal environment or joining material might be required. We designed a customizable three-way joint, as shown in Fig 16. (a) left. Considering easy and universal assembly, we embedded high cavity ratio *TF-Cells* near every joint's inlet hole. Next, to allow bending, we embedded *Simple Beam* to the joint's body. As the joint body is a large cross-section ($23 \times 23\text{(mm)}$), we made the central part of the body ($10 \times 10\text{(mm)}$) as hollow and embedded *TF-Cells* and five *Solid* beam shape into the non-hollow parts, as shown in Fig 16. (a) left. Through heating the *TF-cells* embedded inlet, solid wood pieces with arbitrary cross-section were tightly inserted into each inlet. Then, we heated the cells in the body and adjusted the joint angle, as shown in Fig 16. (a) right.

7.2 Ergonomic Fitting: glasses and screw gripper

Thermoforming through *TF-Cells* can continuously modify 3D printed objects until they ergonomically fit users. We fabricated two examples:

glasses and a screw gripper. The size of the glasses is bigger than our print bed. Moreover, the geometry of the glasses requires a large supporter for printing. We made flat and small glasses as shown in Fig 16. (b). At this time, we simply embedded a *Helix* into bridges and embedded *Simple Beams* into the tips and hinges for refining. First, the tips were heated to twist 90° and the angle refined to fit to the ears. Similarly, the hinges were thermoformed to find an appropriate angle. Finally, the length of bridges was slightly adjusted according to the distance between the eyes (Fig 16. (b)). We designed a screw gripper that tightly holds a screw and ergonomically fitted it to a user hand, as shown in Fig 16. (c) left. We roughly made a screw shape hole and embed low density *TF-cells*. Then, we embedded a *Helix* into two sections of grip for controlling its length to allow multiple thermoforming with enough sensitivity. We also embedded a *Horizontal Array* into the rear section to adjust grip's angle. Through thermoforming the assembly part, we assemble the screw tightly into the gripper. Initially, we reduced the length by heating and pressing the second *Helix* section but re-fit grip by heating and stretching the first *Helix* section. Finally, we ergonomically fitted the grip's angles, as in Fig 16. (c) right.

7.3 Aesthetic Tuning: low-poly-Pikachu and 3D peace gesture hand

TF-Cells allow users to tune 3D object for aesthetic purposes. Besides, thermoforming can be used for modifying an open source *STL* file with multiple constraints for modification in the modeling stage [2]. As illustrated in Fig 1, we downloaded *Low-Poly Pikachu* from Thingiverse [8] and tuned its posture by thermoforming *TF-Cells* in its neck. Modeling an organic 3D shape is challenging and takes significant time. Thermoforming *TF-Cells* could address the difficulties, like our 3D peace hand gesture. To make a 3D hand giving a peace sign, we drew a 2D hand and simply extruded. Next, we embedded *Simple Beam* into the thumb, ring finger (two sections for middle and proximal phalanx), and pinky for folding. We also put *Vertical Array* in the wrist for slightly twisting and bending. After heating all the embedded parts, we deformed each part and smoothed them for finishing. Finally, we could modify the flat hand into a 3D hand with peace gesture as shown in Fig 16. (d) right.

8 DISCUSSION

8.1 Extension of Using *TF-Cells*

Although we focused on the PCL filament, the main principle of *TF-Cells* can be used to thermoform other filaments like PLA. To adapt PLA, its shape changing effects and safety should be considered. When we heated PLA to 200 °C, the structures became self-deformed around 80°C, which blocks half of the cavity. For heating, hot water can also be a usable source. When inserting *TF-Cells* into 90 °C water, *TF-Cells* were particularly heated to a malleable state with less blocked front cavity. Although it is challenging to control heat, it can be a possible source.

8.2 Safety Issue

We heated *TF-Cells* to 80 °C for PCL. Human skin is known to get thermally injured when in contact with a relatively low temperature of 55 °C for a minute or more [21]. Thus, directly deforming an object should be conducted carefully with thermally-resistant gloves or tools. Fortunately, the temperature of the section 5 mm above the heating spot was at most 34 °C and was thus safe to grasp. On the contrary, during heating, it is not recommended to handle the objects with bare hands, particularly when the hot air has a high velocity [27].

8.3 Repeatability and Working Time

Thermoforming through *TF-Cells* is difficult to repeat. As heating blocks the perforated structure of *TF-Cells*, reheating the cells is ineffective; it is similar to heating *Conventional*. One solution is embedding *TF-Cells* into multiple regions for deforming, as aforementioned, with the screw gripper. Otherwise, users need to deform during the limited working time (i.e., the time the cells are in the malleable state). Fortunately, the working time might be sufficient for the modifications. In case of the specimens in Experiment 5, stretching and pressing were possible until 370 s after heating while twisting and bending until 480 s. Also, the time could be extended with additional heating.

8.4 Limitations: perforated appearance and overhang

The perforated appearance of *TF-Cells* is a significant limitation. As the gaps in *TF-Cells* increase, the sizes of the cavities become larger. Bending and stretching also enlarges the cavity size. Thus, using *TF-Cells* might be not appropriate when a smooth surface is required. Regarding this issue, it is useful to bring extra mass from other parts and flatten the surface with tools. The printability of *TF-Cells* is also a limitation. While enlarging the gap is beneficial for thermoforming, it also enlarges overhang where parts of beams protrude, which could reduce the printing quality. Thus, it is necessary to counterbalance the printing quality and heat transference.

9 CONCLUSION AND FUTURE WORK

In this study, we introduced *TF-Cells* which can facilitate thermoforming, such as stamping, fitting, and four shape modifications. To provide standards and directions for using *TF-Cells*, we technically investigated them through a series of experiments. Further, we presented several examples of compound cells, which solve some of

the issues when manipulating shapes through *TF-Cells*. Adopting the resulting data, we designed a simple design tool for embedding *TF-Cells* into 3D models. We provided applicable contexts with five examples. Finally, we discussed limitations and extension of *TF-Cells*. For future scope, further exploration of compound cells with multi-material printing and developing a user-friendly design tool could be studied. In addition, *TF-Cells* in 4D printing contexts might be explored such as diverse self-actuate deformation and designing actuating moment by controlling the thermal conductivity of an object.

ACKNOWLEDGMENTS

We appreciate Youngkyou Kim of Korea Conformity Laboratories for the technical measurement of material properties. We would like to acknowledge the technical support from ANSYS Korea.

REFERENCES

- [1] [n.d.]. eMate-PCL filament—White | eSUN 3D Printing Materials. <http://www.esun3d.net/products/292.html>
- [2] Celena Alcock, Nathaniel Hudson, and Parmit K. Chilana. 2016. Barriers to Using, Customizing, and Printing 3D designs on Thingiverse. *Proceedings of the International ACM SIGGROUP Conference on Supporting Group Work* 13–16–Nove, September (2016), 195–199. <https://doi.org/10.1145/2957276.2957301>
- [3] Byoungkwon An, Hsiang-Yun Wu, Teng Zhang, Lining Yao, Ye Tao, Jianzhe Gu, Tingyu Cheng, Xiang 'Anthony' Chen, Xiaoxiao Zhang, Wei Zhao, Youngwook Do, and Shigeo Takahashi. 2018. Thermorph: Democratizing 4D Printing of Self-Folding Materials and Interfaces Byoungkwon. In *Conference on Human Factors in Computing Systems - Proceedings*. Association for Computing Machinery (ACM), 1–12. <https://doi.org/10.1145/3173574.3173834>
- [4] Marie-Pierre -P Bertin, Gérard Marin, and Jean-Pierre -P Montfort. 1995. Viscoelastic properties of acrylonitrile-butadiene-styrene (ABS) polymers in the molten state. *Polymer Engineering & Science* 35, 17 (1995), 1394–1406. <https://doi.org/10.1002/pen.760351711>
- [5] Hal F. Brinson, L. Catherine Brinson, Hal F. Brinson, and L. Catherine Brinson. 2015. Characteristics, Applications and Properties of Polymers. In *Polymer Engineering Science and Viscoelasticity*. Springer US, 57–100. https://doi.org/10.1007/978-1-4899-7485-3_3
- [6] Sungmin Cho, Yunsil Heo, and Hyunwoo Bang. 2012. Turn: A virtual pottery by real spinning wheel. *ACM SIGGRAPH 2012 Posters, SIGGRAPH'12* 234, July 1987 (2012), 1997. <https://doi.org/10.1145/2342896.2342911>
- [7] Richard V Craster and Sébastien Guenneau. 2012. *Acoustic metamaterials: Negative refraction, imaging, lensing and cloaking*. Vol. 166. Springer Science & Business Media.
- [8] FLOWALISTIK. 2014. Low-Poly Pikachu. <https://www.thingiverse.com/thing:376601>
- [9] Kosta Grammatikos. 2020. How to Make a 3D Printed Mask - COVID-19 Pandemic | Raise3D. <https://www.raise3d.com/case/how-to-make-a-3d-printed-mask-during-the-covid-19-pandemic/>
- [10] Daniel Groeger, Elena Chong Loo, and Jürgen Steimle. 2016. HotFlex: Post-print customization of 3D prints using embedded state change. *Conference on Human Factors in Computing Systems - Proceedings* (2016), 420–432. <https://doi.org/10.1145/2858036.2858191>
- [11] Tovi Grossman, Ravin Balakrishnan, and Karan Singh. 2003. An interface for creating and manipulating curves using a high degree-of-freedom curve input device. *Conference on Human Factors in Computing Systems - Proceedings* 5 (2003), 185–192.
- [12] Dale Hayward. 2019. Bone mother: The challenges of making an indie 3d printed film. *ACM SIGGRAPH 2019 Talks, SIGGRAPH 2019* (2019). <https://doi.org/10.1145/3306307.3328142>
- [13] Liang He, Huaishu Peng, Michelle Lin, Ravikanth Konjeti, François Guimbretière, and Jon E. Froehlich. 2019. Ondulé: Designing and Controlling 3D Printable Springs. In *UIST 2019 - Proceedings of the 32nd Annual ACM Symposium on User Interface Software and Technology*. Association for Computing Machinery, 739–750. <https://doi.org/10.1145/3332165.3347951>
- [14] Megan Hofmann, Kristin Williams, Toni Kaplan, Stephanie Valencia, Gabriella Hann, Scott E. Hudson, Jennifer Mankoff, and Patrick Carrington. 2019. "Occupational Therapy is Making": Clinical Rapid Prototyping and Digital Fabrication Megan. (2019), 1–13. <https://doi.org/10.1145/3290605.3300544>
- [15] Ken ichi Kameyama. 1997. Virtual clay modeling system. *ACM Symposium on Virtual Reality Software and Technology, Proceedings, VRST* (1997), 197–200.

- [16] Alexandra Ion, Johannes Frohnhofer, Ludwig Wall, Robert Kovacs, Mirela Alistar, Jack Lindsay, Pedro Lopes, Hsiang-Ting Chen, and Patrick Baudisch. 2016. Metamaterial Mechanisms. *Proceedings of the 29th Annual Symposium on User Interface Software and Technology - UIST '16* (2016), 529–539. <https://doi.org/10.1145/2984511.2984540>
- [17] Alexandra Ion, Robert Kovacs, Oliver S. Schneider, Pedro Lopes, and Patrick Baudisch. 2018. Metamaterial textures. In *Conference on Human Factors in Computing Systems - Proceedings*, Vol. 2018-April. 1–12. <https://doi.org/10.1145/3173574.3173910>
- [18] Alexandra Ion, Ludwig Wall, Robert Kovacs, and Patrick Baudisch. 2017. Digital mechanical metamaterials. *Conference on Human Factors in Computing Systems - Proceedings* 2017-May (2017), 977–988. <https://doi.org/10.1145/3025453.3025624>
- [19] Hiroki Kaimoto, Junichi Yamaoka, Satoshi Nakamaru, Yoshihiro Kawahara, and Yasuaki Kakehi. 2020. Expand fab: Fabricating objects expanding and changing shape with heat. *TEI 2020 - Proceedings of the 14th International Conference on Tangible, Embedded, and Embodied Interaction* (2020), 153–164. <https://doi.org/10.1145/3374920.3374949>
- [20] W Karwowski. 2006. *International Encyclopedia of Ergonomics and Human Factors-3 Volume Set*. CRC Press. https://books.google.com/books?hl=en&lr=&id=Ih-z6lkTO8EC&oi=fnd&pg=PP1&dq=International+Encyclopedia+of+Ergonomics+and+Human+Factors++Volume+Set&jots=oUorulfVgX&sig=wBTnI8Wc{ }_sDEokzG-3zsiHOxtM
- [21] E. H. Leach, R. A. Peters, and R. J. Rossiter. 1942. Experimental Thermal Burns, Especially the Moderate Temperature Burn. *Quarterly Journal of Experimental Physiology and Cognate Medical Sciences* 32, 1 (1942), 67–86. <http://doi.wiley.com/10.1113/expphysiol.1943.sp000875>
- [22] David Ledo, Fraser Anderson, Ryan Schmidt, Lora Oehlberg, Saul Greenberg, and Tovi Grossman. 2017. Pineal: Bringing Passive Objects to Life with Embedded Mobile Devices. In *Conference on Human Factors in Computing Systems - Proceedings*, Vol. 2017-May. Association for Computing Machinery, 2583–2593. <https://doi.org/10.1145/3025453.3025652>
- [23] Youn-Kyung Lim, Erik Stoltzman, and Josh Tenenberg. 2008. The anatomy of prototypes: Prototypes as filters, prototypes as manifestations of design ideas. *ACM Transactions on Computer-Human Interaction* 15, 2 (jul 2008), 1–27. <https://doi.org/10.1145/1375761.1375762>
- [24] G. MCCLAREN. 1998. Abstracting Craft: The Practiced Digital Hand. *Journal of Design History* (1998). <https://doi.org/10.1093/jdh/11.1.102>
- [25] Stefanie Mueller, Pedro Lopes, and Patrick Baudisch. 2012. Interactive Construction: Interactive Fabrication of Functional Mechanical Devices. In *Proceedings of the 25th annual ACM symposium on User interface software and technology - UIST '12*. ACM Press, New York, 599. <https://doi.org/10.1145/2380116.2380191>
- [26] Stefanie Mueller, Anna Seufert, Huaishu Peng, Robert Kovacs, Kevin Reuss, François Guimbretière, and Patrick Baudisch. 2019. Formfab: Continuous interactive fabrication. In *TEI 2019 - Proceedings of the 13th International Conference on Tangible, Embedded, and Embodied Interaction*. Association for Computing Machinery, Inc, New York, NY, USA, 315–323. <https://doi.org/10.1145/3294109.3295620>
- [27] T. Panitz and D. T. Wasan. 1972. Flow attachment to solid surfaces: The Coanda effect. *AIChE Journal* 18, 1 (1972), 51–57. <https://doi.org/10.1002/aic.690180111>
- [28] Gwanwoo Park, Sunggu Kang, Howon Lee, and Wonjoon Choi. 2017. Tunable multifunctional thermal metamaterials: Manipulation of local heat flux via assembly of unit-cell thermal shifters. *Scientific Reports* 7, December 2016 (2017), 1–15. <https://doi.org/10.1038/srep41000>
- [29] Huaishu Peng, Jimmy Briggs, Cheng Yao Wang, Kevin Guo, Joseph Kider, Stefanie Mueller, Patrick Baudisch, and François Guimbretière. 2018. Roma: Interactive fabrication with augmented reality and a Robotic 3D printer. *Conference on Human Factors in Computing Systems - Proceedings* 2018-April (2018). <https://doi.org/10.1145/3173574.3174153>
- [30] Huaishu Peng, Amit Zoran, and François Guimbretière. 2015. D-Coil : A Hands-on Approach to Digital 3D Model Design. *Conference on Human Factors in Computing Systems - Proceedings* (2015), 1807–1815.
- [31] Austin A. Phoenix and Evan Wilson. 2018. Adaptive thermal conductivity metamaterials: Enabling active and passive thermal control. *Journal of Thermal Science and Engineering Applications* 10, 5 (2018), 1–9. <https://doi.org/10.1115/1.4040280>
- [32] Muhammad Raza, Yichao Liu, El Hang Lee, and Yungui Ma. 2016. Transformation thermodynamics and heat cloaking: A review. *Journal of Optics (United Kingdom)* 18, 4 (2016). <https://doi.org/10.1088/2040-8978/18/4/044002>
- [33] Andrew O. Sagerman-Furnas, Nobuyuki Umetani, and Ryan Schmidt. 2015. Meltables: Fabrication of complex 3D curves by melting. *SIGGRAPH Asia 2015 Technical Briefs, SA 2015* Figure 2 (2015). <https://doi.org/10.1145/2820903.2820915>
- [34] Valkyrie Savage, Ryan Schmidt, Tovi Grossman, George Fitzmaurice, and Björn Hartmann. 2014. A Series of Tubes: Adding Interactivity to 3D Prints Using Internal Pipes. In *UIST 2014 - Proceedings of the 27th Annual ACM Symposium on User Interface Software and Technology*. Association for Computing Machinery, Inc, 3–12. <https://doi.org/10.1145/2642918.2647374>
- [35] Martin Schmitz, Martin Herbers, Niloofar Dezfuli, Sebastian Günther, and Max Mühlhäuser. 2018. Off-line sensing: Memorizing interactions in passive 3D-printed objects. In *Conference on Human Factors in Computing Systems - Proceedings*, Vol. 2018-April. Association for Computing Machinery, New York, New York, USA, 1–8. <https://doi.org/10.1145/3173574.3173756>
- [36] Martin Schmitz, Jürgen Steimle, Jochen Huber, Niloofar Dezfuli, and Max Mühlhäuser. 2017. Flexibles: Deformation-aware 3D-printed tangibles for capacitive touchscreens. *Conference on Human Factors in Computing Systems - Proceedings* 2017-May (2017), 1001–1014. <https://doi.org/10.1145/3025453.3025663>
- [37] Christian Schüller, Daniele Panozzo, Anselm Grundhöfer, Henning Zimmer, Evgeni Sorkine, and Olga Sorkine-Hornung. 2016. Computational thermoforming. *ACM Transactions on Graphics* 35, 4 (2016), 1–9. <https://doi.org/10.1145/2897824.2925914>
- [38] Lingyun Sun, Jiaji Li, Yu Chen, Yue Yang, Ye Tao, Guanyun Wang, and Lining Yao. 2020. 4DTexture: A Shape-Changing Fabrication Method for 3D Surfaces with Texture. (2020), 1–7. <https://doi.org/10.1145/3334480.3383053>
- [39] Lingyun Sun, Yue Yang, Yu Chen, Jiaji Li, Guanyun Wang, Ye Tao, and Lining Yao. 2020. ShrinkyKit: 3D Printing Shrinkable Adaptations for Everyday Objects. (2020), 1–7. <https://doi.org/10.1145/3334480.3383034>
- [40] Rundong Tian, Vedant Saran, Mareike Kitzler, Florian Michahelles, and Eric Paulos. 2019. Turn-by-wire: Computationally mediated physical fabrication. *UIST 2019 - Proceedings of the 32nd Annual ACM Symposium on User Interface Software and Technology* (2019), 713–725. <https://doi.org/10.1145/332165.3347918>
- [41] Skylar Tibbits. 2014. 4D printing: Multi-material shape change. *Architectural Design* 84, 1 (2014), 116–121. <https://doi.org/10.1002/ad.1710>
- [42] Nirzaree Vadgama and Jörgen Steimle. 2017. Flexy: Shape-customizable, single-layer, inkjet printable patterns for 1d and 2d flex sensing. *TEI 2017 - Proceedings of the 11th International Conference on Tangible, Embedded, and Embodied Interaction* (2017), 153–162. <https://doi.org/10.1145/3024969.3024989>
- [43] Marynel Vázquez, Eric Brockmeyer, Ruta Desai, Chris Harrison, and Scott E. Hudson. 2015. 3D Printing Pneumatic Device Controls with Variable Activation Force Capabilities. In *Conference on Human Factors in Computing Systems - Proceedings*, Vol. 2015-April. Association for Computing Machinery, 1295–1304. <https://doi.org/10.1145/2702123.2702569>
- [44] K. P. Vemuri, F. M. Canbazoglu, and P. R. Bandaru. 2014. Guiding conductive heat flux through thermal metamaterials. *Applied Physics Letters* 105, 19 (2014), 103–107. <https://doi.org/10.1063/1.4901885>
- [45] Kiril Vidimčić, Alexandre Kaspar, Ye Wang, and Wojciech Matusik. 2016. Foundry: Hierarchical material design for multi-material fabrication. *UIST 2016 - Proceedings of the 29th Annual Symposium on User Interface Software and Technology* (2016), 563–574. <https://doi.org/10.1145/2984511.2984516>
- [46] Guanyun Wang, Ye Tao, Ozguc Bertug Capunaman, Humphrey Yang, and Lining Yao. 2019. A-line: 4D Printing Morphing Linear Composite Structures. *Conference on Human Factors in Computing Systems - Proceedings* (2019), 1–12. <https://doi.org/10.1145/3290605.3300656>
- [47] Christian Weichel, John Hardy, Jason Alexander, and Hans Gellersen. 2015. ReForm: Integrating Physical and Digital Design through Bidirectional Fabrication. *UIST '15 Proceedings of the 28th Annual ACM Symposium on User Interface Software & Technology* (2015), 93–102.
- [48] Christian Weichel, Manfred Lau, David Kim, Nicolas Villar, and Hans W. Gellersen. 2014. MixFab: A Mixed-Reality Environment for Personal Fabrication. (2014), 3855–3864. <https://doi.org/10.1145/2556288.2557090>
- [49] Karl D.D. Willis, Cheng Xu, Kuan-Ju Wu, Golan Levin, and Mark D. Gross. 2011. Interactive fabrication. (2011), 69. <https://doi.org/10.1145/1935701.1935716>
- [50] Karl D. D. Willis, Eric Brockmeyer, Scott E. Hudson, and Ivan Poupyrev. 2012. Printed Optics: 3D Printing of Embedded Optical Elements for Interactive Devices. In *UIST '12: Proceedings of the 25th annual ACM symposium on User interface software and technology*. Association for Computing Machinery (ACM), 589–598. <https://doi.org/10.1145/2380116.2380190>